

## Chapter 2

# High-Resolution THz Spectroscopy of Biomolecules and Bioparticles: Concentration Methods

E.R. Brown, W. Zhang, L.K. Viveros, E.A. Mendoza, Y. Kuznetsova, S.R.J. Brueck, K.P. Burris, R.J. Millwood, and C.N. Stewart

**Abstract** During the past several years we have utilized fluidic-chip and waveguide-concentrator technology in combination with high-resolution frequency-domain THz spectroscopy to detect absorption signatures in biomolecules and bioparticles of various types, especially the nucleic acids and bacterial spores. Some of the signatures have been surprisingly narrow ( $<20$  GHz FWHM), leading to the hypothesis that the fluidic chips can enhance certain vibrational resonances because of their concentrating and linearizing effects. For solid or moist bio-samples, circular waveguide coupling allows signature detection of small quantities with some degradation of sensitivity but no loss of resolution. It concentrates the radiation, not the biomaterial. This method was used to demonstrate strong THz signatures in bacterial spores (e.g., *Bacillus thuringiensis*).

**Keywords** THz radiation • THz coherent spectroscopy • Vibrational signatures • Nucleic-acid molecules • Lambda DNA • Nanofluidic chips • Circular waveguide concentrator • Conical horns • *Bacillus thuringiensis*

---

E.R. Brown (✉)

Wright State University, Dayton, OH, USA

Physical Domains, LLC, Glendale, CA, USA

e-mail: [elliott.brown@wright.edu](mailto:elliott.brown@wright.edu)

W. Zhang • L.K. Viveros

Wright State University, Dayton, OH, USA

E.A. Mendoza

Redondo Optics, Inc., Redondo Beach, CA, USA

Y. Kuznetsova • S.R.J. Brueck

Center for High Technology Materials and Department of Electrical and Computer Engineering, and Physics and Astronomy, University of New Mexico, Albuquerque, NM, USA

K.P. Burris • R.J. Millwood • C.N. Stewart

Department of Plant Sciences, University of Tennessee, Knoxville, TN, USA

## 2.1 Background

THz radiation remains of great interest for biomolecular sensing because it interacts resonantly with collective vibrations that involve hundreds or more atomic constituents. They are therefore more specific to the *primary structure* of the biomolecules, compared to the interatomic vibrations sensed by traditional IR spectroscopy (e.g., FTIR). In addition, THz is inherently non-ionizing to biomolecules, and like IR spectroscopy, can detect “label free” targets. Sub-THz vibrational modes in the nucleic acids DNA and RNA have been investigated for several decades going back to seminal work by Van Zandt [1] and Wittlin [2]. The former emphasized the existence of sub-THz polar optical phonon modes in aqueous DNA, while the latter emphasized an optically active hydrogen bond between the base pairs. Later, the study of localized vibrational modes became of interest, and in more recent work narrow signatures have been observed [3–4].

## 2.2 Introduction

### 2.2.1 Sample Presentation

More recently the importance of sample presentation and concentration has become better appreciated, leading to our investigation of new techniques for THz measurement of biomolecules. This paper reviews two such techniques, displayed schematically in the system block diagram of Fig. 2.1. The first is a nanochannel, fluidic-chip platform for the aqueous nucleic acid samples and proteins. The second technique concentrates the THz radiation into circular metal waveguide structures where vibrations can be excited efficiently in sub-wavelength dry samples, such as powders. The second technique concentrates the THz radiation into circular metal waveguide structures where vibrations can be excited efficiently in sub-wavelength dry-powder or grainy samples. In other words, the first technique is concentrating the biomaterial, and the second technique is concentrating the THz electric field.

### 2.2.2 High-Sensitivity THz Spectrometry

Our spectrometer of choice is the state-of-the-art coherent frequency-domain transceiver shown in Fig. 2.1 [5–7]. Because of spectral and spatial coherence, it is amenable to both sample-presentation techniques just described. Like time-domain spectroscopy, photomixing utilizes ultrafast photoconductive emitters and detectors but driven by single-frequency temperature-tunable distributed-feedback (DFB) semiconductor lasers rather than mode-locked lasers. It provides a continuously tunable coherent tone from below 100 GHz to ~2.0 THz with instantaneous linewidth

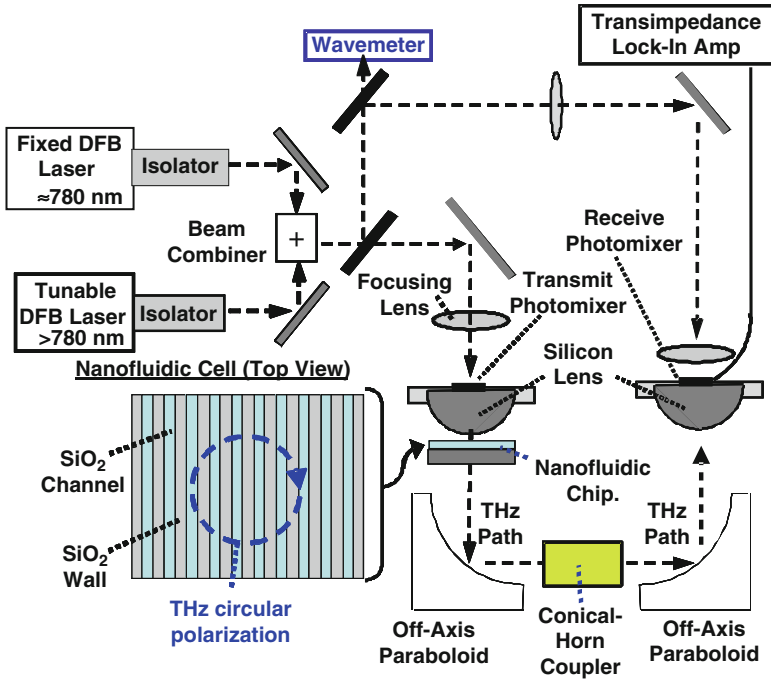


**Fig. 2.1** Block diagram of THz coherent transceiver showing optimum location of the nanofluidic chip adjacent to the transmit photomixer, and the conical-horn waveguide coupler at the middle of the THz path (only one method used at a time)

of  $\sim 100$  MHz or better [8]. The photomixers are fabricated at the center of an ultra-compact planar square-spiral antenna which radiates a primarily circular polarized beam above  $\sim 200$  GHz. Including antenna impedance effects, the bandwidth of each photomixer is approximately 1.0 THz. One photomixer acts as the transmitter and the other acts as the receiver. The radiation from the transmit photomixer is coupled from the antenna to free space through a high-resistivity silicon hyperhemispherical lens. The THz beam is then collimated using an aspherical optic, usually an off-axis paraboloid. The reciprocal process occurs between free space and the receive photomixer.

Because the lasers driving receive and transmit photomixers are mutually coherent, the THz beam into the receive photomixer is mixed down in frequency by homodyne conversion. A simple amplitude modulation on the transmit photomixer then allows for dc offset and straightforward synchronous detection with all the benefits of traditional homodyne transceivers. With no samples in the THz path, this spectrometer produces a high dynamic range, typically in the range 70–80 dB at 100 GHz, and 50–60 dB at 1.0 THz. This range is achieved without evacuation of the free-space portion of the spectrometer so that water-vapor absorption lines do not appear, especially when the ambient humidity is high. Unless one of these water

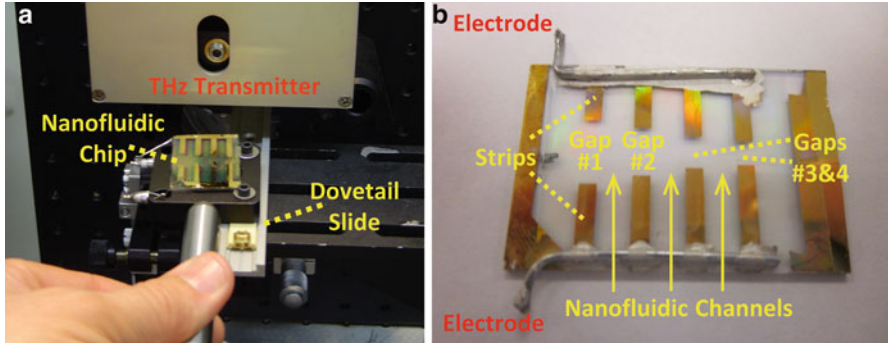


**Fig. 2.2** (a) Fluidic chip lying on precision dovetail slide. (b) Close-up of fluidic chip showing the transparent quartz substrate, metal strips (connected by electrodes), and gaps between the strips through which the THz propagates

vapor lines coincides with a signature from the sample-of-interest, this does not pose a problem. On the contrary, because the water vapor lines are highly resolved, their known shape and strength is often used to monitor the frequency metrology and dynamic range of the instrument.

The samples of interest are mounted in one of the three positions shown in Fig. 2.1. The fluidic chips are usually located at the lens port of the transmit or receive photomixer where the THz beam diameter is  $\approx 3$  mm, which underfills the nanochannel aperture of the chip. As shown in Fig. 2.2a, the chip is mounted on a precision dovetail slide for accurate and repeatable placement in the THz beam path. The circular-waveguide coupler is always located at the half-way point between the transmit and receive photomixers where the beam is collimated with a spot size of  $\approx 1$  cm. The insertion loss of the fluidic chip is  $\approx 2$ – $3$  dB, whereas the waveguide coupler loss is  $>20$  dB. Nevertheless, the waveguide coupler transmits enough power to maintain signal strengths at least  $\sim 20$  dB above the noise floor out to 1.0 THz. This takes advantage of the high-dynamic range of the instrument, which is typically 80 dB at 200 GHz, 60 dB at 1.0 THz, and 40 dB at 1.6 THz.

## 2.3 Sample Methods and Results

### 2.3.1 Fluidic Chips

The intent of the fluidic chips is to concentrate and possibly linearize nucleic-acid molecules in nanochannel arrays, while maintaining efficient coupling to free-space THz radiation. To fabricate the nanochannels at the micron scale and below, we have applied submicron-interference lithography and silica-nanoparticle calcination techniques [9]. In the present samples the channels were approximately 800 nm wide by

1,000 nm deep, on a pitch of  $\sim 1,200$  nm, and separated from opposing reservoirs by about 5 mm. It takes  $\sim 15$  min to fill the channels by capillary action [10], and the filling and concentrating effects have been confirmed by fluorescence imaging [10]. The THz transmission is then measured with the beam aligned at the center of the nanochannel array. The spatially-coherent, focused THz beam is typically 3 mm in diameter, so much smaller than the  $\sim 5 \times 5$ -mm aperture of the fluidic chip.

Historically, this fluidic-chip platform quickly displayed strong signatures in the smaller nucleic-acid samples, such as those for small-interfering RNA shown in Fig. 2.3a [11]. This particular sample was a mixture of 17-, 21-, and 25-bp ds-siRNA molecules. The signatures are the strongest and narrowest ( $< 20$  GHz FWHM) we have ever observed in nucleic acid solutions. And three of them stood out in terms of absorption depth, labeled S1, S2, and S3 in Fig. 2.3a, and centered at 916, 962, and 1,034 GHz, respectively. In the meantime we have searched for signatures of larger molecules, starting with double-stranded DNA in the range between 50 and 1,000 bp. Most of these appeared similar to the transmission spectrum for 50-bp DNA shown in Fig. 2.3b. Three prominent signatures tended to appear between 850 and 1,000 GHz, the three in Fig. 2.3b being centered at  $\approx 870$ , 938, and 993 GHz, and labeled in correspondence with those of si-RNA. Note however that the signatures in Fig. 2.3b are significantly weaker and broader than those of Fig. 2.3a (which is why the vertical scale in Fig. 2.3a is logarithmic and in Fig. 2.3b linear).

The largest nucleic-acid specimen studied to date is Lambda DNA – the bacteriophage for the *Escherichia coli* bacterium, which consists of 48,502 base-pairs [12]. A typical transmission spectrum for Lambda DNA is shown in Fig. 2.3c between 0.8 and 1.1 THz. Again, there are three prominent signatures, but they are even weaker and broader than those in Fig. 2.3b, and not very distinguishable from the typical transmission-spectrum undulations. However, it is compelling to combine all of the center frequencies in Fig. 2.3 to compose the trend chart shown in Fig. 2.4. Here we see the tendency for the center frequency to shift downward between the smallest DNA (17-bp) and the largest (48.5-kbp) tested.

## 2.3.2 Waveguide Concentrator

### 2.3.2.1 Dry Control Sample

The circular-waveguide coupler is displayed in Fig. 2.5a, consisting of two conical horn antennas aligned back-to-back and separated by a thin circular waveguide section located near the throat of each horn. The thin waveguide section contains the biosample with two very thin ( $\sim 12$   $\mu\text{m}$  thick) plastic windows held taut by the waveguide flanges. Because of the high radiative condensing capability of horn antennas, this technique is well suited to coupling limited THz power to a small volume filled with a solid sample. Our first investigation of this method utilized a 500- $\mu\text{m}$ -diameter circular-waveguide section that was 380  $\mu\text{m}$  thick. This corresponds to a sample

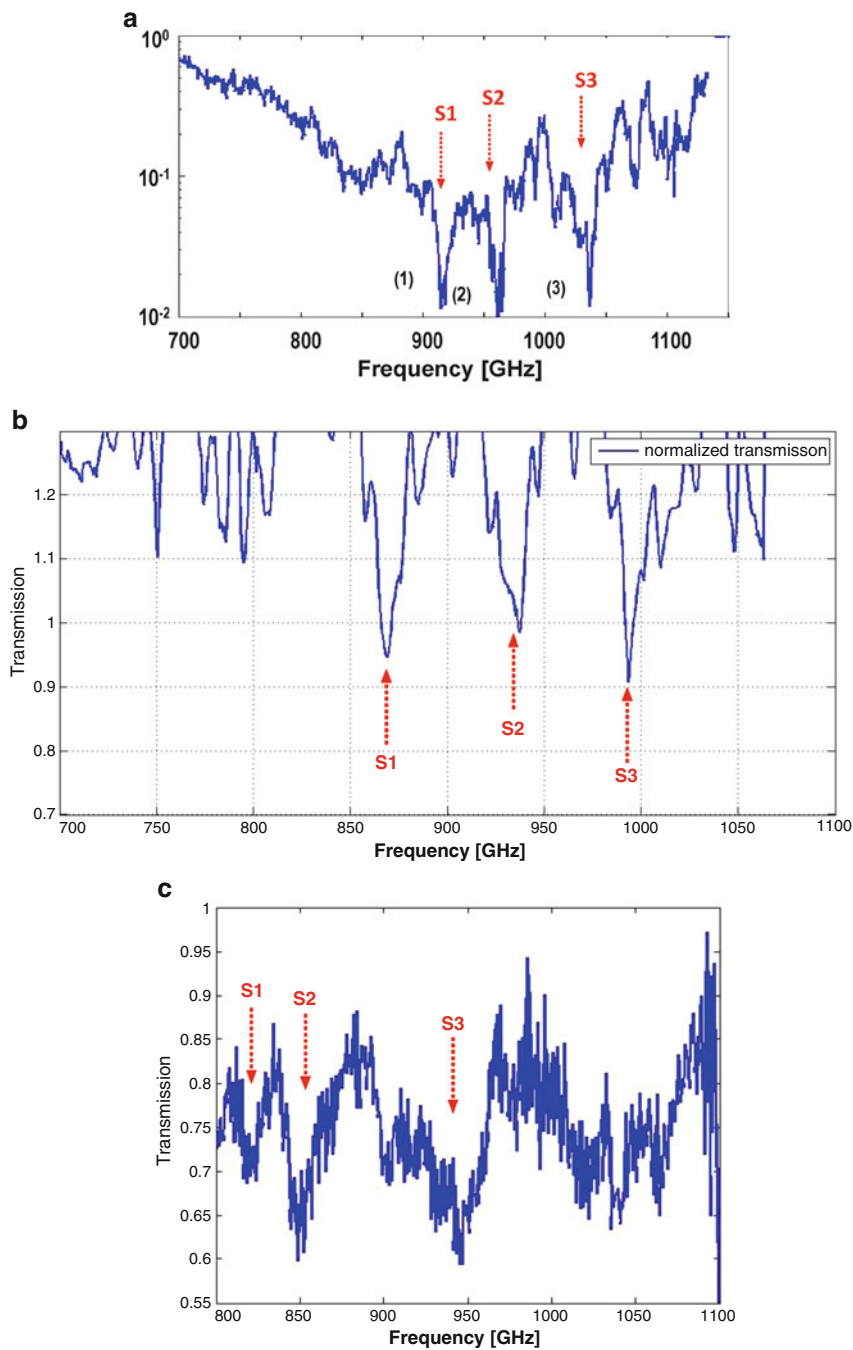


**Fig. 2.3** THz transmission measured through fluidic chips filled with solutions of (a) si-RNA, (b) 50-bp DNA, and (c) Lambda DNA. S1, S2, and S3 denote the strongest signatures, assumed to be common between the three samples

**Fig. 2.4** The three signature center frequencies, S1, S2, and S3 from Fig. 2.3 plotted vs size of the nucleic acid sample in units of base-pairs [bp]

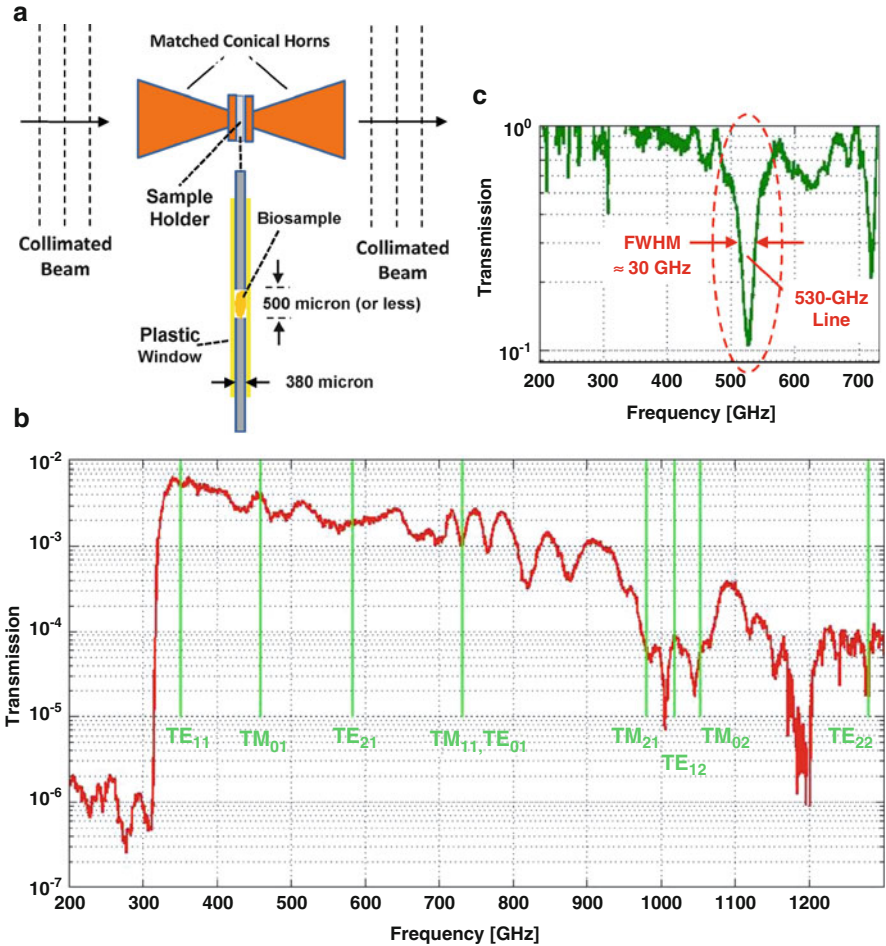
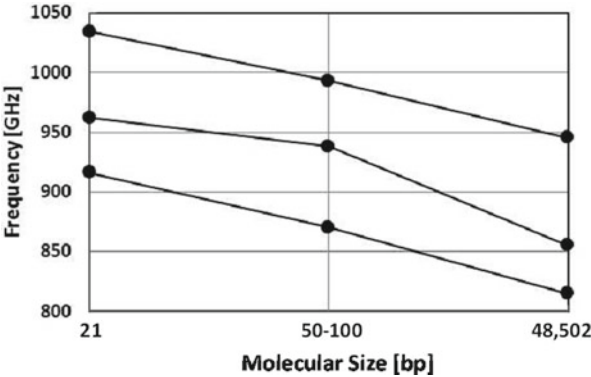


**Fig. 2.5** (a) Exploded view of circular waveguide concentrator with conical horn coupling, (b) Background transmission through waveguide concentrator relative to free-space propagation, (c) Transmission through lactose monohydrate



volume of  $\approx 77 \mu\text{l}$ , which is small enough that dangerous or expensive samples can be used with relative impunity.

The experimental protocol was to start with the horn coupler located as shown in Fig. 2.1 but without any sample, and then measure transmission relative to a background consisting of the open-path spectrum. As always the noise floor was measured with the THz path blocked, resulting in the horn-coupler transmission spectrum shown in Fig. 2.5b. There are two notable aspects of this spectrum. The first is a precipitous turn-on in the transmission around 320 GHz that rises by about 40 dB starting from just above the noise floor. This is the expected cut-off frequency  $f_c$  of the  $\text{TE}_{11}$  mode of the 500- $\mu\text{m}$  diameter circular waveguide at the throat of the horn. Electromagnetic theory [13] predicts this as  $f_c = (1.841/d) * c/(\pi) = 346 \text{ GHz}$ , assuming  $d = 0.020 \text{ in.}$  (508  $\mu\text{m}$ ), the nominal radius of the circular waveguide according to the machine tools used. The discrepancy between the experiment and theory is explained by the machining tolerance of  $\approx +5 \%$ . Adding this to the nominal diameter, we get  $d = 0.021 \text{ in.}$  ( $r = 533 \mu\text{m}$ ), or  $f_c = 330 \text{ GHz}$ , as shown by the vertical dashed line in Fig. 2.5b and in good agreement with experiment.

The second notable aspect is a roll-off in transmission with frequency up to 1.0 THz, and a maximum transmission of only  $\approx 7 \times 10^{-3}$  around 340 GHz. The gradual roll-off in transmission is attributed to excitation of higher-order modes in the circular waveguide. The cut-off frequency for each successive mode is shown in Fig. 2.5b (assuming  $d = 508 \mu\text{m}$ ). The first debilitating drop in transmission occurs around 1.0 THz where the  $\text{TM}_{21}$ ,  $\text{TE}_{12}$  and  $\text{TM}_{02}$  cut-off frequencies are in close proximity. The low maximum transmission is attributed primarily to mismatch and misalignment between the quasi-Gaussian beams in the coherent THz spectrometer and the horn coupler. This misalignment is a consequence of too many degrees-of-freedom. The guided-wave portion of the horn coupler is mounted in a gimbal, so must be adjusted in both azimuth and elevation, which is difficult to optimize. In spite of the mismatch loss, the instrument still produces the radiative concentration effect we seek, and achieves useful transmission levels because of the high dynamic reserve of the coherent photomixing spectrometer.

To demonstrate spectroscopic capability on solids, we filled the circular-waveguide section with lactose monohydrate powder using a needle. The monohydrate-crystallized form of lactose (milk sugar) has become a standard THz absorber because of its two strong and narrow signatures centered at 530 and 1,369 GHz, respectively [14, 15]. In our experiment, the transmission through the lactose was computed relative to a background scan through the empty horn coupler, and to the instrument noise floor. As displayed in Fig. 2.5c, the lactose signature centered at 530 GHz is fully resolved in depth and width. This is believed to be the smallest volume of lactose monohydrate ever detected in the THz region.

### 2.3.2.2 Wet Sample

The interest in THz bacterial spectroscopy started in earnest with the anthrax pathogen (*Bacillus anthracis*) domestic-terror events in the U.S. shortly after 9/11/2001. This event proved that a simple postal letter could disguise the presence



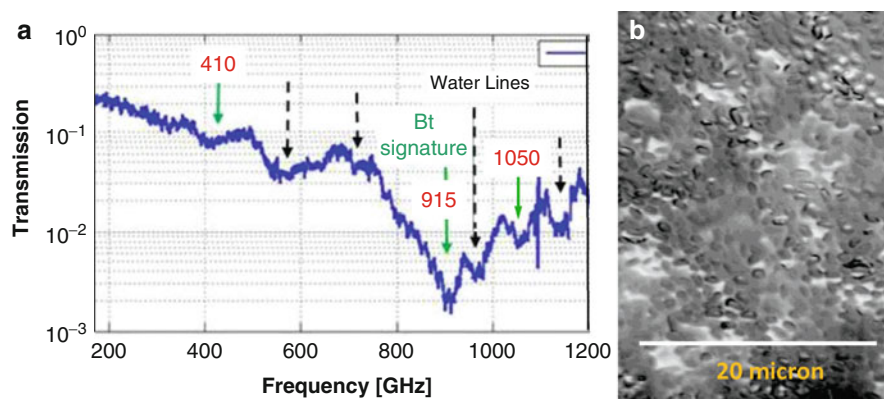


**Fig. 2.6** (a) THz transmission spectrum through *Bacillus thuringiensis* (Bt) paste smeared on filter paper. (b) Scanning electron micrograph of Bt paste

of the deadly anthrax spores from conventional biosensors. The high transparency of paper and similar dry insulating materials to THz radiation begged the question of whether Anthrax offered any radiative signatures. So some experimental studies were conducted on an innocuous Anthrax simulant, *Bacillus subtilis* (Bg), and signatures were measured at or near 415 and 1,035 GHz [16, 17]. However, these signatures were rather weak and difficult to reproduce, in addition to the fact that (Bg) was difficult to obtain outside of a biological laboratory.

Therefore, more recently we investigated another species of genus *Bacillus*, *B. thuringiensis* (Bt), also a candidate surrogate for anthrax, but much easier to obtain and less controlled. In fact, it is a common “green” pesticide used throughout the world, and widely cultured for agriculture and plant sciences. Our first sample had a pasty consistency so was readily smeared into Whatman<sup>TM</sup>-5 filter paper. To our delight, this provided the interesting THz transmission spectrum shown in Fig. 2.6a, with unmistakable and reproducible signatures centered around 410, 915, and 1,050 GHz [18]. The signature at 915 GHz was, in fact, the strongest THz biosignature we had ever measured up to that point. To elucidate the origin of the strong signature, we obtained a scanning-electron micrograph of the sample as shown in Fig. 2.6b. The spores are clearly visible as prolate spheroids, and occupy approximately 50 % of the biomass, the remainder of which is mostly obliterated cell-wall and cytoplasmic material.

To determine whether the signatures in Fig. 2.6a are independent of the filter-paper method, we took a very small amount of the moist, pasty Bt material and located it in the sample holder of the waveguide coupler of Fig. 2.5a. Although tedious and imprecise, the waveguide-coupler was able to maintain the moisture level for a long time (~1 h). We then obtained the spectrum in the lower part Fig. 2.7 showing the strongest signature centered around 910 GHz, which is reduced below that in Fig. 2.6a by more than the frequency uncertainty in our experiment (0.5 GHz). Analysis of this signature has led to its model as a surface-phonon polariton

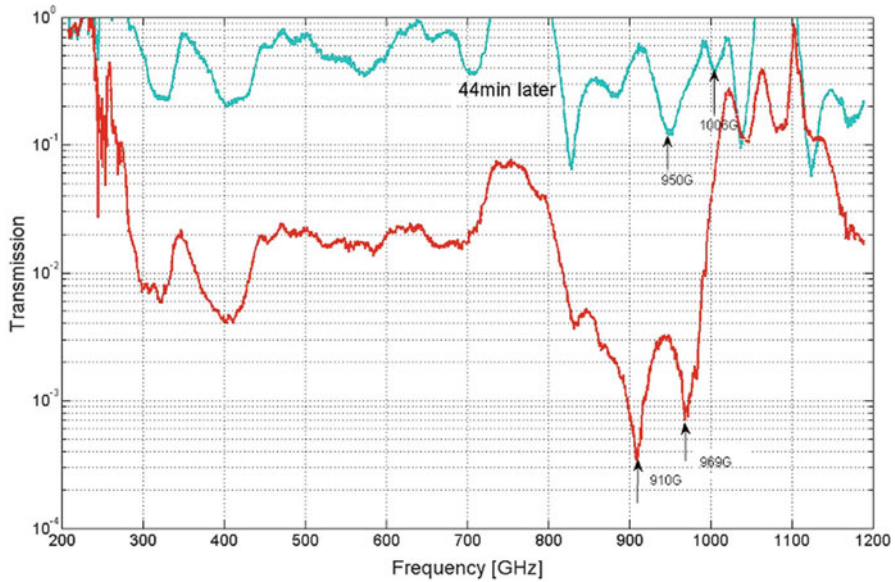


**Fig. 2.7** THz transmission through small quantity of Bt paste in circular waveguide coupler while moist (lower, red), and 44 min later after drying (upper, blue)

resonance on the outer coat of the *Bacillus* spore. Although this was first proposed in 2006 for *B. subtilis* [19], it could never be proven because of the relative weakness of the signatures.

Believing that the hydration level could be responsible for the frequency shift, we maintained the same sample in the waveguide coupler for ~44 min just to dehydrate with no other changes in the experiment. The spectrum shown in the upper part of Fig. 2.7 was obtained. As expected, with less hydration there was significantly higher transmission through the sample across the entire band since liquid water is very absorbing in the THz region. However, to our surprise the strong signature at 910 GHz disappeared, proving that hydration level affects the signature strength significantly. This may also be consistent with the surface-phonon polariton mechanism since in the moist state liquid water will likely bind to the spore coat, polarizing its surface. And when dried, the surface proteins on the spore collapse their normal structure.

## 2.4 Conclusion and Future Work

Our research has focused on the detection of signatures in biomolecules and bioparticles, especially nucleic acids and bacterial particles (i.e., spores). Our quest has been aided significantly by the development of concentration methods both for the biomaterial itself and the THz radiation. The preferred concentration method for

liquid samples has been the fluidic chip fabricated in quartz. This was useful in detecting strong signatures in double-stranded nucleic acids up to 48.5-kbp, although the detectability appears to decrease with molecular size. The preferred radiative concentration method has been the circular waveguide with conical-horn coupling. This was useful in detecting the first signatures in bacterial spores (*B. thuringiensis*) and demonstrating their sensitivity to hydration.

Future work will focus first on improving these sample presentation methods, starting with the use of electrophoresis on the fluidic chips to further concentrate and linearize the biomolecules, and also establish concentration control. The waveguide concentrator will be improved by reducing its insertion loss via quasi-optical (i.e., lens) coupling between the spectrometer THz beam and the conical horns. Then we will be in a position to assess these methods and the associated THz signatures as a viable sensor technology. This must include estimates of the *sensitivity* with respect to sample concentration, and *selectivity* with respect to other signatures and the background clutter that is so pervasive in THz spectroscopy.

**Acknowledgments** This material is based upon work supported by, or in part by, the U. S. Army Research Laboratory and the U. S. Army Research Office under contract numbers W911NF-11-1-0024 and W911NF-11-C-0080.

## References

1. Van Zandt LL, Prohofsky EW, Kohli M (1980) Microwave absorption by double-helical DNA. *Int J Quant Chem Quant Biol Symp* 7:35–38
2. Wittlin A, Genzel L, Kremer F, Häselser D, Poglitsch A (1986) Far-infrared spectroscopy on oriented films of dry and hydrated DNA. *Phys Rev A* 34:493–500
3. Van Zandt LL, Saxena VK (1994) Vibrational local modes in DNA polymers. *J Biomol Struct Dyn* 11:1149
4. Woolard DL, Kosica T, Rhodes DL, Cui HL, Pastore RA, Jensen JO, Jensen JL, Loerop WR, Jacobsen RH, Mittleman D, Nuss MC (1997) Millimeter wave-induced vibrational modes in DNA as a possible alternative to animal tests to probe for carcinogenic mutations. *J Appl Toxicol* 17(4):243–246
5. Verghese S, McIntosh KA, Calawa S, Dinatale WF, Duerr EK, Molvar KA (1998) Generation and detection of coherent terahertz waves using two photomixers. *Appl Phys Lett* 73:3824
6. Bjarnason JE, Brown ER (2005) Sensitivity measurement and analysis of an ErAs:GaAs coherent photomixing transceiver. *Appl Phys Lett* 87:134105
7. Demers JR, Logan RT Jr., Bergeron NJ, Brown ER (2008) A coherent frequency-domain THz spectrometer with a signal-to-noise ratio 60 dB at 1 THz. In: *Proceedings of the SPIE, Paper# 6949-8*, Orlando, 16–20 March 2008
8. Brown ER, Bjarnason J, Chan TLJ, Driscoll DC, Hanson M, Gossard AC (2004) Room temperature, THz photomixing sweep oscillator and its application to spectroscopic transmission through organic materials. *Rev Sci Instrum* 75:5333
9. Xia D, Brueck SRJ (2005) Fabrication of enclosed nanochannels using silica nanoparticles. *J Vac Sci Tech B* 23:2694–2699
10. Xia D et al (2008) DNA transport in hierarchically-structured colloidal nanoparticle porous-wall nanochannels. *Nano Lett* 8:1610–1618
11. Brown ER, Mendoza EA, Xia D-Y, Brueck SRJ (2010) Narrow THz spectral signatures through DNA and RNA in nanofluidic channels. *IEEE Sensors J* 10(755)

12. Sanger F, Coulson AR, Hong GF, Hill DF, Petersen GB (1982) Nucleotide sequence of bacteriophage  $\lambda$  DNA. *J Mol Biol* 162(4):729–773
13. Pozar DM (2005) *Microwave engineering*, 3rd Ed. Wiley, Hoboken, NJ
14. Brown ER, Bjarnason JE, Fedor AM, Korter TM (2007) On the strong and narrow absorption signature in lactose at 0.53 THz. *Appl Phys Lett* 90:061908
15. Roggenbuck A, Schmitz H, Deninger A, Camara Mayorga I, Hemberger J, Gusten R, Gruninger M (2010) Coherent, broadband continuous-wave THz spectroscopy on solid-state samples. *New J Phys* 12:043017
16. Globus TR, Woolard DL, Khromova T, Crowe TW, Bykhovskaia M, Gelmont BL, Hesler JL, Samuels AC (2003) THz-spectroscopy of biological molecules. *J Biol Phys* 29:89–100
17. Brown ER et al (2004) Optical attenuation signatures of *Bacillus Subtilis* in the THz region. *Appl Phys Lett* 84(18):3438–3440
18. Zhang W, Brown ER, Viveros L, Burris K, Stewart N (2013) Narrow terahertz attenuation signatures in *Bacillus thuringiensis*. *J Biophoton*. doi:[10.1002/jbio.201300042](https://doi.org/10.1002/jbio.201300042)
19. Brown ER, Khromova TB, Globus T, Woolard DL, Jensen JO, Majewski A (2006) THz regime attenuation signatures in *Bacillus subtilis* and a model based on surface polariton effects. *IEEE Sens J* 6(5):1076–1083

Terahertz and Mid Infrared Radiation: Detection of  
Explosives and CBRN (Using Terahertz)

Pereira, M.; Shulika, O. (Eds.)

2014, XIII, 196 p. 103 illus., 70 illus. in color., Hardcover

ISBN: 978-94-017-8571-6